An application of FEA and machine learning for the prediction and optimisation of casing buckling and deformation responses in shale gas wells in an in-situ operation.

MOHAMMED, A.I., BARTLETT, M., OYENEYIN, B., KAYVANTASH, K. and NJUGUNA, J.

2021

An application of FEA and Machine Learning for the Prediction and Optimisation of Casing Buckling and Deformation Responses in Shale Gas Wells in an In-situ Operation

Auwalu I Mohammed[1], Mark Bartlett[2], Babs Oyeneyin[3], Kambiz Kayvantash[4], James Njuguna[1]
[1]Centre for Advanced Engineering Materials, School of Engineering, Robert Gordon University, Garthdee Road, Aberdeen UK
[2]School of Computing Science and Digital Media, Robert Gordon University, Garthdee Road, Aberdeen UK
[3]I-Flow Energy Holdings Ltd, 17 Kedslie Road, Edinburgh UK EH16 6NT
[4]CADLM, 32 rue Victor Baloche, 91320 Wissous, Paris, France

Abstract

This paper proposes a novel way to study the casing structural integrity using two approaches of finite element analysis (FEA) and machine learning. The approach in this study is unique, as it captures the pertinent parameters influencing the casing buckling and the evaluation of the magnitude of each. In this work, the effect of combined loading using multiple parameters to establish the relationship and effect of each on stress, displacement and ultimately casing safety factor is revealed.

The optimised result show remarkable improvement in reducing the total deformation, the von Mises and increasing the safety factor of the casing under combined loading condition. The optimised casing shows 89% reduction in total deformation and 87% reduction in von Mises in comparison to unoptimised simulation result. In addition, the safety factor of 3.3 is obtained against the initial predicted stress of 932.46 MPa with a corresponding safety factor of 0.8129.

Real time parametric prediction and optimisation using Lunar and Quasar (ODYSSEE software package) enabled the examination of the casing structural responses based on the pertinent parameters. In effect, a very good agreement was found between "KNN" and Lunar predictions on parameters influencing casing buckling phenomena and the corresponding Mises stress. Lunar optimisation provided the ideal parameter values for the attainment of pre-define von Mises stress as a function of other factors. This quick approach shows both accuracy and validation of the two independent procedures arriving at the same conclusion. We found that concurrent investigation of the casing buckling attributing factors and optimisation using FEA and ODYSSEE package is sufficient to maintain casing structural integrity during shale gas extraction process.

Key words: Casing deformation, Shale gas well, Prediction, Optimisation, Machine learning, Artificial Intelligence

1. Introduction

Advances in horizontal well drilling and hydraulic fracturing is now enabling the extraction of shale gas and oil in commercial quantities. However, during shale gas fracturing process (stimulation), the interaction of hydraulic fractures and rock formation is buckling and even shearing the steel casing leading to lack of access into the well and costly delays in drilling out bridge plugs in the process (Jacobs 2020; Guo et al. 2018; Xing et al. 2017; Lian et al. 2017). In more severe cases, this can lead to complete loss of access to the lateral section of the wells. The

casing failure under this circumstance is considered to be intra-well phenomena that can take several forms and has no universal driver.

The literature has documented some of the major reasons attributed to the casing buckling and deformation phenomena based on field experience from notable shale gas provinces. For example, in China - Xi et al. (2019) pointed out that fault slippage in multistage fracturing caused casing shear failure. Also, according to Xi et al. (2018) and Wang et al. (2018) fracturing activates pre-existing fractures that lead to casing shear buckling. Analysis of casing failures in the Granite Wash play in the western Anadarko Basin also identified poor cementing to be responsible for casing buckling (Carpenter 2019).

However, Lin et al. (2017) established that rock mechanical strength reduces most in Longmaxi Formations at a slip angle of 45^0 and continue to be destabilised with increase in number of stimulated stages along the lateral section of the wells. As a result, the casing structural integrity is compromise which translate to lack of access into the wells to drill-out bridge plugs. The casing stresses are further amplified due to thermal and pressure in volume fracturing of shale gas wells (Xi et al. 2018). In addition, Haghshenas et al. (2017) and Liu et al. (2017) pointed out that casing deformation is due to imposed additional load by fracture slip and weak bedding plane through the wellbore in the process of hydraulic fracturing. The studies of Mohammed et al. (2020) and Yin et al. (2018) show that creep load (slippage) lead to an increase of transverse displacement and stresses on the casing.

According to Yu et al. (2019) overlapping, asymmetric stimulated zones in adjacent stages effectively increase the resultant shear force on the casing that may lead to its failure ("S" shaped deformations). Besides, Lian et al. (2015) and Wang (2016) attributed casing buckling to fluctuations in in- situ stresses as a result of fracturing pressure. Furthermore, Mohammed et al. (2019) review on casing failure pointed that the casings are subjected to material degradation due to perforations, varying local loads - in situ stresses, induced stresses due to stimulation, natural fracture activation and propagation, slip and shear during their installation and operation leading to different kinds of casing failure modes.

In contrast, different countermeasures are being proposed in the literature corresponding to specific scenarios to avoid casing failures. For example, simulation results on shale gas horizontal wells suggest avoiding natural fractures and nearby faults during shale gas stimulation can reduce casing failure (Guo et al. 2018). Furthermore, using cement with an elastic modulus smaller than 10GPa and higher casing grade can significantly reduce casing buckling phenomena in such wells (Guo et al. 2018). However, Zhang et al. (2020) pointed out that casing grade and cement sheath thickness have limited impact on casing deformation. While a new analytical study by Liu et al. (2020) developed a model for the prediction of time dependent stresses and pore pressures near the wellbore.

In addition, Yin et al. (2018) investigated casing shear deformation induced by fracture slip during multistage hydraulic fracturing in a particular well in China. The study established that increasing casings' flexural strength does not prevent deformation. However, low slip angle and using cement with low elastic modulus is minimising the potentials of casing failure phenomenon (Guo et al. 2018; Yin et al., 2018; Xi et al., Yan et al., 2019). Meanwhile, Yan et al. (2019) suggested that

reducing the fracturing pressure is sufficient to maintained casing integrity during stimulation process. The study of Lian et al. (2015) and Lin et al. (2017) indicated that the key to solving casing deformation and/or buckling is reasonable spacing in the design of multi- stage hydraulic fracturing.
The established procedure in the design of casing for oil and gas wells involves casing grade selection and an estimation of the various loads expected to occur on the casing with some safety margin based on predicted downhole conditions of that particular well. However, this procedure is inadequate and cannot be generalised to adequately meet the design requirement for shale gas wells where casing –cement and formation rock are bonded together with induced stresses during fracturing.

These propositions are case specific and cannot be generalised to address casing buckling phenomena as noted above. Therefore, in this study, finite element modelling (FEM) is conducted together with design exploration using ANSYS design explorer and Lunar to determine the relationship between the main attributing parameters. In addition, using Lunar, Quasar and machine learning approaches, strength and weakness of the parameters that are sensitive to casing buckling in the process of shale gas wells hydraulic fracturing are evaluated and optimisation performed to guide future casing selection and design strategy in shale gas well development.

As noted above, despite designing of the casing for shale gas wells, during shale gas stimulation, the interaction of hydraulic fracturing and formation geomechanics is buckling and shearing the casing leading to buckling and deformation. Hence, different finite element modelling has been conducted (see Figure 4 for an overview) to evaluate the structural responses of the casing in shale gas wells covering static and dynamic situations. The significance of these modelling is to circumvent the limitation of conventional design to predict the casing responses and aggregate the various scenarios of finite element modelling (FEM) for optimisation using machine learning.

2. The casing Buckling/Deformation Phenomena

As pointed above, the casing deformation phenomena is a combination of more than one attributing factor (Mohammed et al., 2019). The predominant factor is often depended on the casing specific failure mode. The complex inter-relationship between these factors remains an engineering challenge to engineers and researchers in tackling this problem during shale gas horizontal wells development. For instance, Yu et al., (2019) presented a complicated casing buckling failure owing to in-situ stress and stress re-distribution during shale gas well development. This is presented in Figure 1. The stress keeps on increasing from stage 8-10 as shown. After the 10^{th} stage, the P110 casing grade is permanently deformed reaching a maximum of 773.8MPa (Yu et al., 2019).

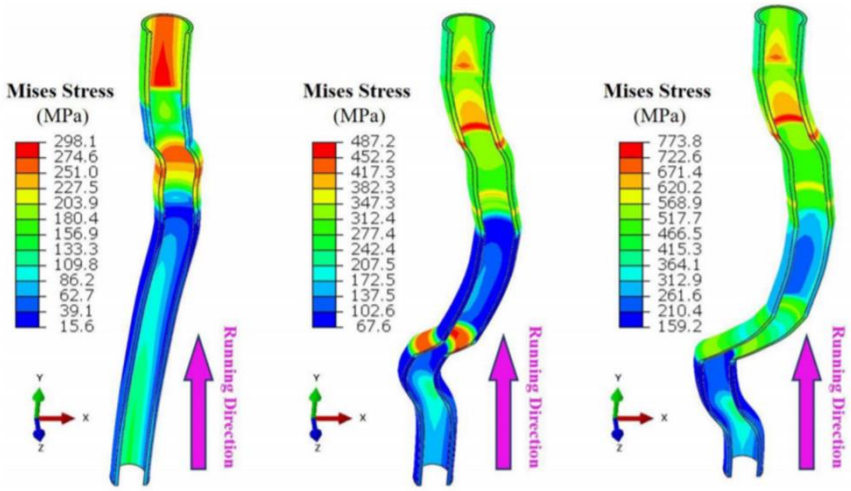

Figure 1: XY-1 well: Casing buckling in shale gas horizontal well located in Sichuan Basin, China (Yu et al., 2019).

The magnitude of the microseismic moment is usually in the range of 2–4 as established by Bao and David, (2016). However, Yan et al., (2019) pointed out that exceptional microseism appeared on fault groups, indicating that the fault is activated during multistage fracturing. Further analysis into the well section that experience unique microseismic moment, corresponds to casing shear failure as shown on Figure 2. As it can be seen on Figure 2, the section of the casing associated with fault slip is buckled while the section that is not is "intact" as shown.

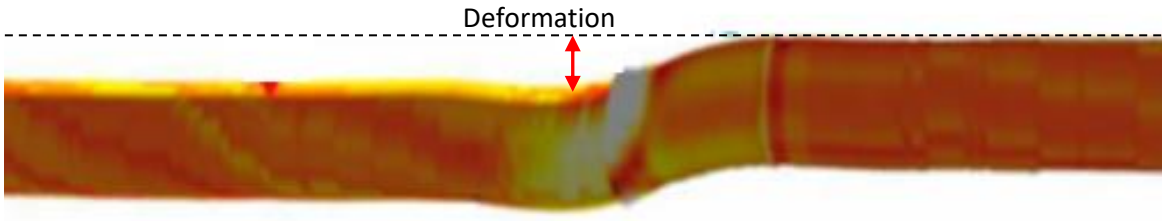

Figure 2 actual casing shear deformation based on microseismic data (Yan et al. 2019).

Figure 3 (a and b) presents the relationships between microseismic moment magnitude, fault radius and slip distance calculated based on analysis by (Yan et al., 2019). It can be seen on Figure 3(a and b) that the increase in the degree of microseismic moment magnitude, the radius and slip distance increases; with the increase of stress drop, the radius decreases, and the slip distance increases (Yan et al., 2019). Microseismic data from an actual shale gas well was used to verify the accuracy of this approach by Yan et al., (2019).

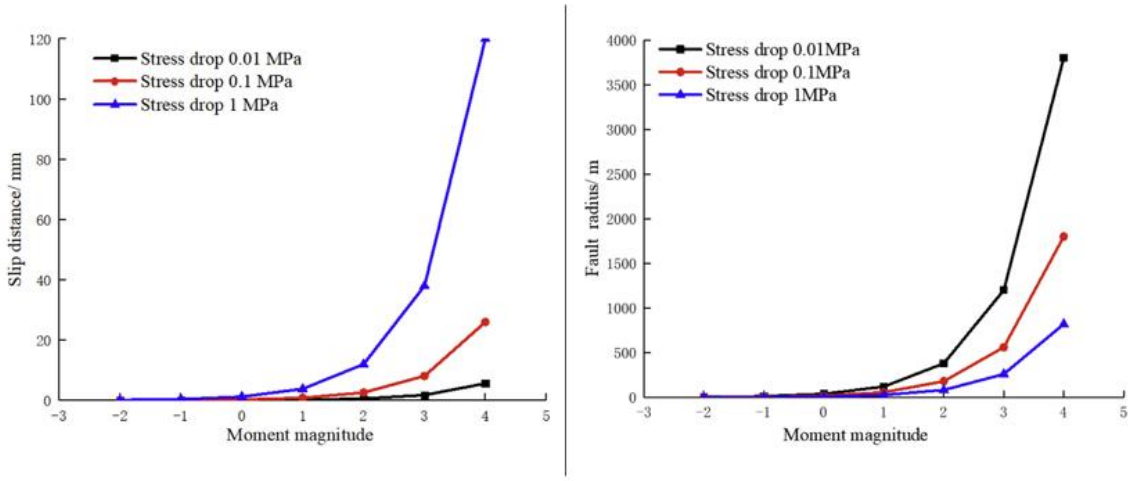

Figure 3:(a) Moment magnitude against slip distance (b) Moment magnitude against fault radius (Yan et al. 2019).

3. Methodology

The design explorer component of ANSYS Workbench could help to simplify complex designs efficiently and make more robust prediction, parameterisation and optimisation. Using "what if analysis" different designs were carried-out to study the P110 casing grade responses. The computed results are used as the basis for parameter correlation.

In addition, the local sensitivity of an input parameter relative to the output can be establish using "parameter correlation tool". Parameter correlation tool uses Latin Hypercube sampling to ensure even distribution with no repetition of the design points. It can be used to determine what parameter matter and what do not in a design. The correlation can be positive, negative or neutral. Based on this analysis one can horn to a specific objective and/or target in the design and get rid of the attributes that do not matter without compromising the safety of the structure (casing).

The initial simulation takes into consideration the influence of a combined loading of thermal and slip displacement to determine the effect of temperature difference between surface and the downhole (reservoir). Moreover, 5mm slip displacement is assumed to occur during flowback period of 30 hours.

Figure 4 presents a flowchart on the overview implemented in this study. As it can be seen, different modelling (FEM 1-3) which cover both static and dynamic conditions with multiple boundary conditions in each case was simulated. This is followed by design exploration, correlation and sensitivity analysis. This led to generation of 517 simulation scenarios as shown on Figure 4. Using ANSYS design explore tool, a direct optimisation is conducted, and sample result presented on page 17 (Figures 14 and 15).

On the other hand, machine learning prediction and optimisation is carried out using KNN algorithm and ODDYSSEE package.

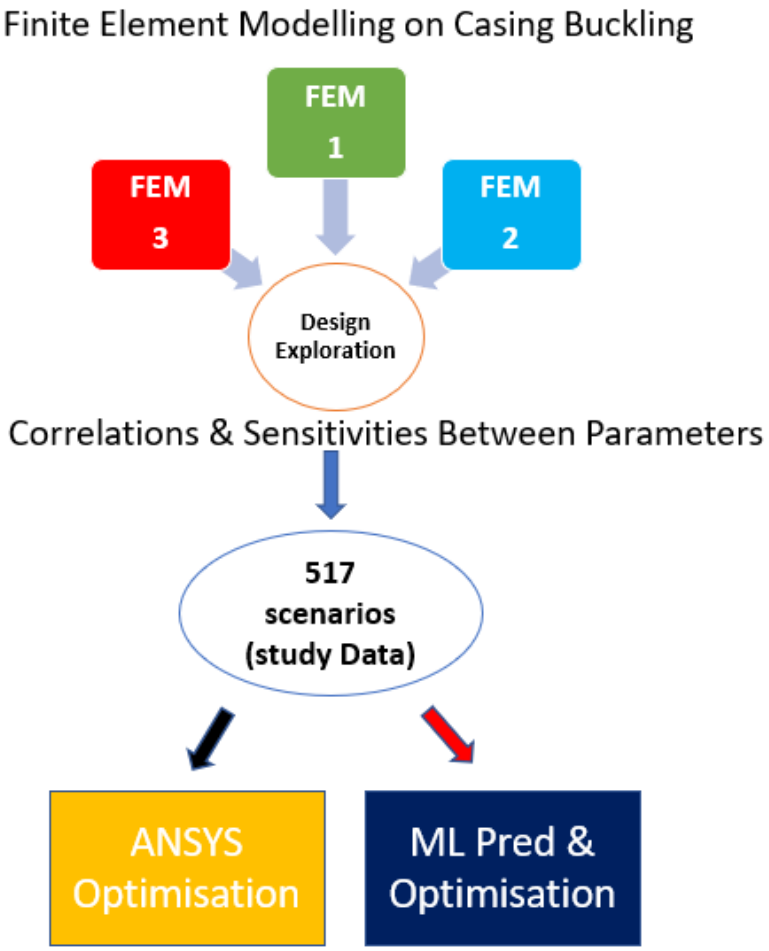

Figure 4 Flowchart on the overview of the study method showing top to down sequence of activities.

3.1 Finite Element Modelling (FEM)

The numerical modelling in this study is an advancement of the previous work by Mohammed et al. (2020). The objective is to predict critical displacement, von Mises stresses and the applicable safety factor in order to establish robust design for the casing as a function of hole dimeter, cement mechanical properties (Elastic modulus and Poisson's ratio), surface and downhole temperatures, slip plane angle and casing geometry.

Simulation results for lateral displacements are in good agreement as per the study of Yin et al. (2018) with less than 5% error accounting for geometric and material nonlinearity as shown on Figure 5.

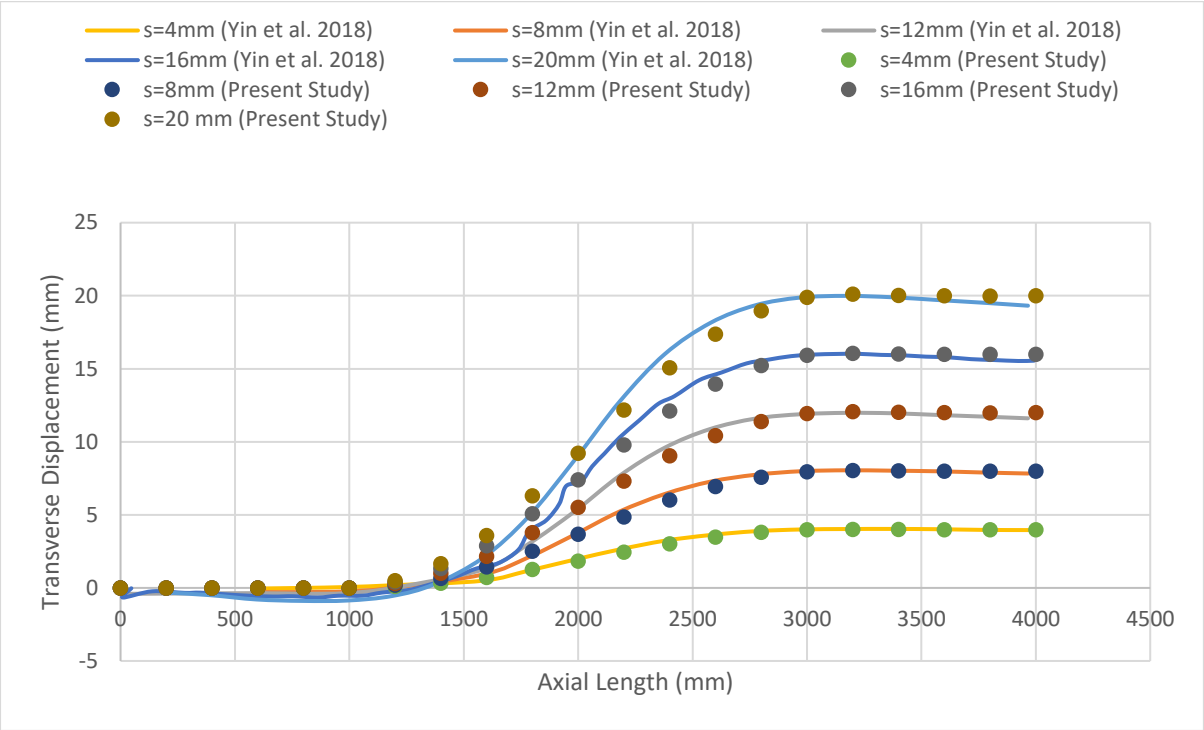

Figure 5 Sample result comparison for validation showing transverse displacement against casing axial length.

The 3D computed aided design (CAD) models comprises of the casing, cement and shale rock is shown on Figure 6. As it can be seen, the shale rock is distinctively separated by the slip plane. The shale rock has a square cross-section with a dimension of 599.95mm to avoid boundary effect on stress and displacement.

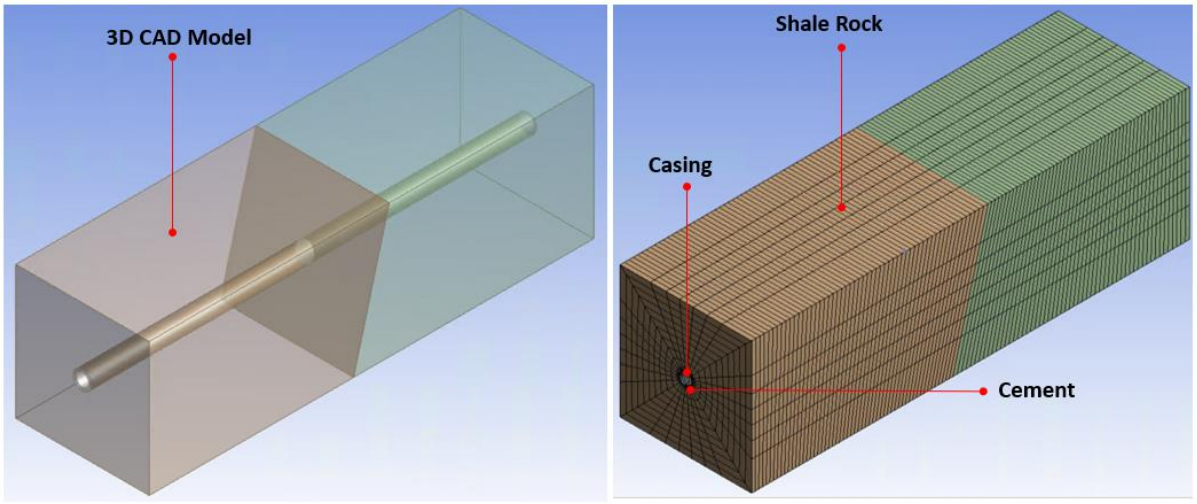

Figure 6 3D CAD and Mesh Models showing casing, cement and shale rock

The element type chosen for this analysis is 'SOLID186'. This is a higher order 3D, element which exhibit quadratic displacement behaviour. This element supports plasticity, large deflection, and strains with mixed formulation capabilities for simulating deformations in layered and homogenous solid materials.

The material properties for the casing, cement and the shale rock for the initial simulation scenario are presented in Table 1.

Table 1 casing, cement, and rock material properties

Materials	Elastic Modulus (MPa)	Poisson's Ratio (μ)	Coefficient of Thermal Expansion (°/C)	Casing Outer Diameter (mm)
P110 Casing Grade	210000	0.3	6.9 X 10 $^{-6}$	139.9
Cement	7000	0.23	9.2 X 10 $^{-6}$	168.275
Shale Rock	20900	0.18	1 x 10 $^{-5}$	-

A bonded relationship is established between the casing, cement, and the rock formation to mimic -rock- cement-casing bonding and to simulate casing structural response under this situation. Buckling under thermal loading with zero displacement (static) is carried out to predict casing response owing to variation between surface and reservoir temperature. Additionally, the same scenario is simulated with a consideration of slip displacement (dynamic). Furthermore, hundreds of simulations are performed to cover wide range of possible scenarios to establish the prevailing factor to the buckling phenomena.

A 5mm displacement was applied on the shale rock to account for the flowback (fault slip activation) after stimulation and to predicts its effect on the casing. Based on this loading, the mechanics of a composites system (casing, cement, and shale rock) and in particular the structural responses of the casing are investigated.

The ANSYS design explorer has demonstrated a robust design as established in this study with improve design factors under combined loading for the casing. Table 2 presents the range of input parameters utilised in the screening optimisation. The novelty of this approach is the concurrent investigation of the main factors attributing to casing buckling phenomena as opposed to previous studies of investigating individual attribute (parameter).

As stated above, the ANSYS design explorer can simplify and optimise structural designs which can be carried out using either screening optimisation, multi-objective genetic algorithm (MOGA) and goal driven optimization method. However, for simplification and making use of good computational resources; the screening optimisation method is selected. This is a simple approach based on sampling and sorting. It supports multiple objectives and constraints as well as all types of input parameters.

Table 2 range of input parameters for the optimisation

Input Parameters	Lower Bound	Upper Bound
Coefficient of Thermal Expansion (C^-1)	8.28E-06	1.012E-05
Cement Modulus (MPa)	6500	10000
Cement Poisson's Ratio	0.207	0.4
Reservoir Temperature (C)	60	250
Ambient Temperature (C)	10	45

Fracturing Pressure (MPa)	30	90
Slip Displacement (mm)	-5.5	-2.75
Slip Plane (degree)	30	75
Inner Diameter (in)	4.05	4.95
Outer Diameter (in)	4.95	5.5
Cement Diameter (in)	5.9625	7.2875
Hole Diameter (in)	5.9625	7.2875

As it can be seen in Table 2 twelve attributes (parameters) are investigated simultaneously to estimate the influence of each on casing buckling phenomena.

Each attribute (parameter) covers wide range of conditions as shown in Table 2. For instance, casing diameter ranges from 4.05inches(102.89mm) to 4.95inches (125.73mm). Similarly, the outer diameter ranges from 4.95 (125.73mm) to 5.5inches (139.70mm), fracturing pressure from 30 to 90MPa. The cement elastic modulus is kept below 10000MPa based on studies (Guo et al. 2018; Yin et al., 2018; Xi et al., Yan et al., 2019) that established making use of cement with low elastic modulus reduces the potentials of casing buckling.

3.2 Data Mining and Machine Learning

Machine learning is the use of a machine/computer to learn in analogy to how the brain learns and predicts. It combines statistics and computer science techniques and depends on a new class of learning algorithms that improve with time, as well as the availability of large datasets to train the systems.

In some cases, the methods are directly inspired by the way the brain works, as is the case with neural networks (Theodoridis, 2015). According to Mitchell (2006) machine learning is defined as a well modelled learning problem - where a computer programme learns from experience (E) with respect to some tasks (T) and some performance measure (P) if its performance on (T) as measured by (P) increase with experience (E). Figure 7 presents schematic diagram of how the machine learning task is accomplished. As it can be seen on Figure 6, machine learning involves two distinct phases, namely the training and the inference or testing phase on a very basic level.

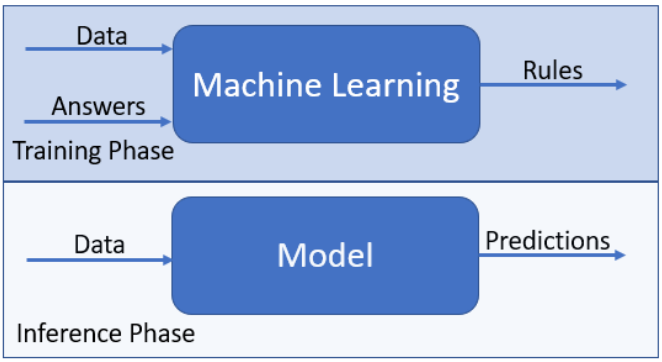

Figure 7 schematic diagram of machine learning task showing the distinct phases between training and testing phase (inference phase).

The first step in manipulating any machine learning task is the depiction of each pattern in the computer (Duda et al. 2012; Talebi et al. 2015; Bartlett and Cussens

2017). This is achieved during the pre-processing stage; where one has to "encode" related information that resides in the raw data in an efficient and information-rich way. This is usually done in a process called data transformation. The raw data in a new space with each pattern represented by a vector, $x \in R^l$. This is known as the feature vector, and its "l" elements are known as the features. In this way, each pattern becomes a single point in l-dimensional space, known as the feature space or the input space. This is referred to as feature generation stage.

Based on the training data, one then designs a function, *f*, which predicts the output label given an input. Once the model has been designed, the system is ready for predictions. Given an unknown pattern, we form the corresponding feature vector, x, from the raw data, and we plug this value into the classifier; depending on the value of *f* (x) (usually on the respective sign, $\hat{y} = sgn\, f(x)$) the pattern is classified in one of the two classes as shown on Figure 8(a).

Two problems at the heart of machine learning task are the classification and regression. The classifier has been designed in order to separate the training data into the two classes (Figure 8a), having on its positive side the points coming from one class and on its negative side those of the other. The 'red' point, whose class is unknown, is classified to the same class as the 'star' points, since it lies on the positive side of the classifier as shown. The goal in classification is to assign an unknown pattern to one out of a number of classes that are considered to be known. For example, in casing deformation, using known scenarios of casing deformations we can classify a new scenario as either deform or undeform (intact).

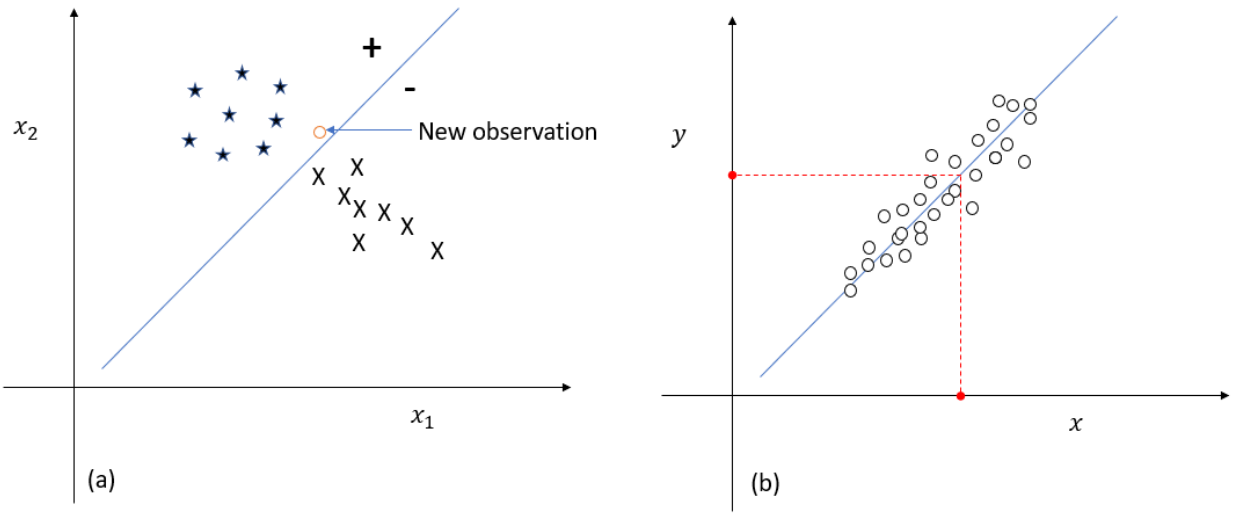

Figure 8: (a) classification (b) regression

Similarly, regression shares to a large extent the feature of classification at preprocessing stage, however, the output variable, y, is not discrete but it takes values in an interval in the real axis or in a region in the complex numbers plane. The regression task is basically a curve fitting problem (Duda et al. 2012). This is usually done by transforming the raw data in a new space with each pattern represented by a vector, $x \in R^l$. This is known as the feature vector, and its *l*

elements are known as the features. In this way, each pattern becomes a single point in an *l*-dimensional space, known as the feature space or the input space.This is referred to as the feature generation stage. For a given a set of training points, $(y_n, x_n)\ y_n \in R, x_n \in R^l, n = 1,2, \dots, N,$ and the task is to estimate a function, f , whose graph fits the data. Once we have found such a function, when an unknown point arrives, we can predict its output value. This is shown in Figure 8b.

3.2.1 Data Mining Using "R"

Like any other machine learning tasks, the relevant libraries deployed in this study include caret, pRoc, mlbench and ggplots2 using results of finite element analysis study in Section 3.1. The classification and Regression Training ("caret") package contains functions to streamline the model training process for complex regression and classification problems. The pROC package contains tools for visualising, smoothing and comparing receiver operating characteristic (ROC curves). The basic unit of the pROC package is the 'ROC' function. It will build a ROC curve, smooth it, if requested (if smooth=TRUE), compute the area under the curve AUC (if auc=TRUE), the confidence interval (CI) if requested (if ci=TRUE) and plot the curve if requested (if plot=TRUE). The mlbench library converts X (which is basically a list) to a data frame. Lastly, the ggplot2 library initializes a ggplot object. It can be used to declare the input data frame for a graphic and to specify the set of plot aesthetics intended to be common throughout all subsequent layers unless specifically overridden.

The "K" Nearest Neighbour Method (KNN) is utilised in this study in that k-nearest neighbour classification for test set from training set looks at each row of the test set, using distances such as Euclidean or Manhattan. The training set vectors are found, and the classification is decided by majority vote, with ties broken at random. If there are ties for the kth nearest vector, all candidates are included in the vote.

On the other hand, the k nearest neighbour regression (knnreg) is utilised which returns the average values of the neighbours. The default value of k is 5, however this parameter has been modified to improve the regression analysis in order to arrive at the most accurate predictive model.

One of the most significant advantages of kNN is that it is relatively easy to implement and interpret (Duda et al. 2012., Theodoridis 2015). Also, with its approach to approximate complex global functions locally, it can be a powerful predictive model. The weaknesses are that kNN is very sensitive to the curse of dimensionality. This refers to scenarios with a fixed size of training examples but an increasing number of dimensions and range of feature values in each dimension in a high-dimensional feature space (Donoho et al. 2000). It can be expensive to compute with a O *(n)* prediction step however, smart implementations and use of data structures such as "K" dimensional-trees and Ball-trees can make kNN substantially more efficient (Donoho et al. 2000; Duda et al., 2012). In general, compared to other machine learning algorithms, the kNN algorithm has relatively few hyperparameters, namely k and the distance metric; however, the choice of an appropriate distance metric is not always obvious. This is because the

performance of the KNN algorithm is dependent on the distance/similarity measure used (Prasatha et al., 2017).

However, using pragmatic approach, numerical modelling and machine learning techniques were applied to evaluate quantitatively the magnitude of these factors under a combined loading scenario. Using "K" nearest neighbour (KNN) machine learning algorithm the simulation data is further studied to establish a predictive model for the von Mises stress. The 517 simulation (instances) is divided into training and testing in the ratio of 70:30, respectively. Preliminary data manipulation involved removing noise and missing values. This is followed by data partitioning in the ratio state above and normalisation. Training and testing are next and finally finetuning the hyper-parameter "k" to establish the best model for the prediction of von Mises stress.

3.2.2 Data Mining and Machine learning for critical deformations

The Lunar is an Artificial Intelligent (AI) software platform that utilised different solvers to perform real time parametric simulation interactively to make prediction and optimisation. Lunar uses past experiences (results) in order to predict new responses with ROM methods (Reduced Order Model method). In contrast, Quasar is a web-based machine learning software that is used for prediction and forecasting (Kayvantash 2019). Specifically, in the Lunar and Quasar the parametric prediction and optimisation this study utilised 258 instances which represent 50% of the simulation data for the training set. On the other hand, the testing set comprises of 129 instances which represent 25% of the simulation data. Furthermore, the relevant data associated with casing (Design of experiment - DOE) and the corresponding responses are predicted, and optimisation performed to determine parameter sets for a desired target. This analysis in Lunar is carried out using the simplified workflow shown in Figure 9.

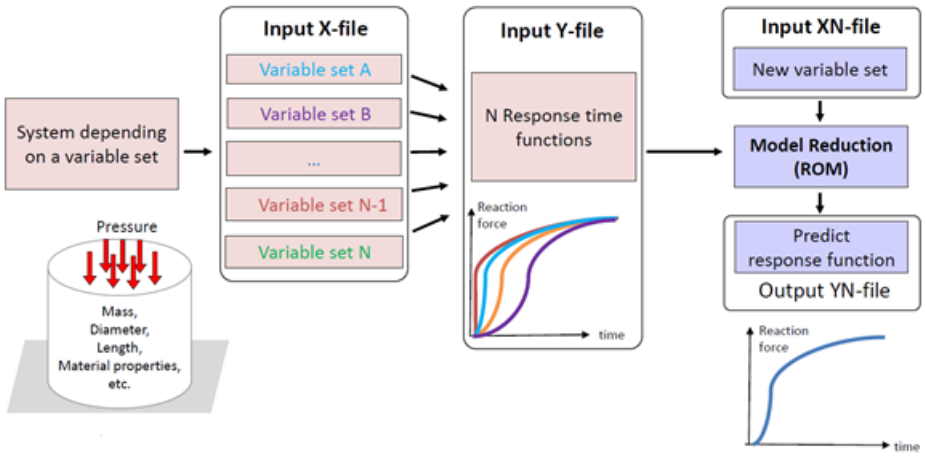

Figure 9 An Overview of Lunar Workflow (Source: CADLM 2019) showing system data bank, input variable (X, Y), and new variable XN.

Additional data modelling in Quasar (machine learning package) is performed using principal component analysis (PCA) to determine the distribution of the sample's designs. The variance of attributing parameters is computed and plotted to estimate how these attributes are diminishing. Furthermore, matrix concatenation operation is carried out on the DOE datasets and the corresponding responses for the generation of heatmap of von Mises stress on the casing.

4. Results and Discussion

4.1 FE simulation results

The results for the combined loading of slip displacement and thermal loading when the fracture slip plane is 60° reveal casing transverse displacement and von Mises stress to be 13.029 mm and 932.46 MPa respectively after 30 hours of combined loading. This is as shown on Figure 10. Under this loading condition the casing is plastically failed since the yield strength of this casing is 758MPa.

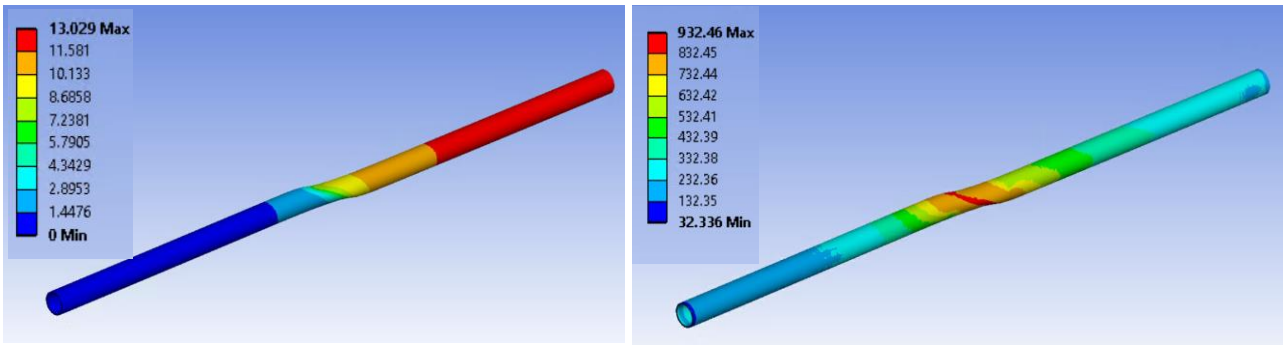

Figure 10 Transverse displacement and von Mises stress after 30 hours of combined loading.

In contrast, the predicted critical transverse displacement and von Mises stress is attained after 9 hours of combined loading. Figure 11 represents contour plots of critical displacement and von Mises stress on the casing under combine loading. Based on these results the casing failure looms after 9 hours of combined loading as shown. Therefore, using design explorer, we work out the optimum design based on the pertinent parameters earlier explained.

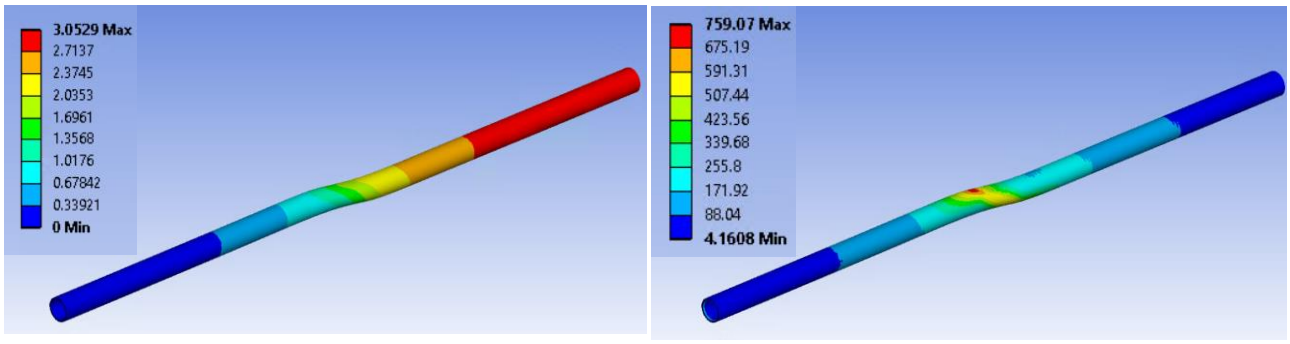

Figure 11 Transverse displacement and von Mises stress after at critical time of cobined loading.

As shown on correlation matrix (Figure 12), slip displacement is negatively correlated to deformation and von Mises. While safety factor minimum is positively correlated with slip displacement as shown. Additionally, slip plane has a neutral

relationship with von Mises stress and safety factor as shown. The red colour codes on the diagonal denotes strong correlation of the same parameter. For example, coefficient of thermal expansion is 1 to 1 correlation (horizontal and vertical), and as such the colour code is red as shown the top left of the correlation matrix. The 12 input parameters are casing coefficient of thermal expansion, cement Young's Modulus and Poisson's ratio. The reservoir temperature (thermal condition magnitude), surface temperature, fracturing pressure (pressure magnitude), slip displacement, slip plane, inner and outer diameter of the casing. Other parameters are cement and well diameter (Hole Diameter). On the other hand, the output parameters are casing von Mises stress, transverse displacement and safety factor.

Furthermore, the local sensitivity of the pertinent parameters is evaluated and plotted on Figure 13. It indicates that hole diameter affects casing deformation positively. Increase in inner diameter, fracturing pressure drives von Mises stress to increase. However, increase in outer diameter reduces the von Mises stress and total deformation, respectively.

The casing geometry is a factor that affects the stress in the casing as can be seen on the local sensitivity chart (Figure 13). Increase in inner diameter reduce the pipe thickness which in turn increase the von Mises stress. Also, fracturing pressure increase the downhole stress which results in increase in von Mises stress. However, increase in outer diameter make the pipe thicker and reduces the von Mises stress accordingly. 32MPa fracturing is moderate which ensure moderate slip displacement on the casing and consequently the stress in the casing remains well below the yield strength 299MPa and 0.76mm transverse displacement.

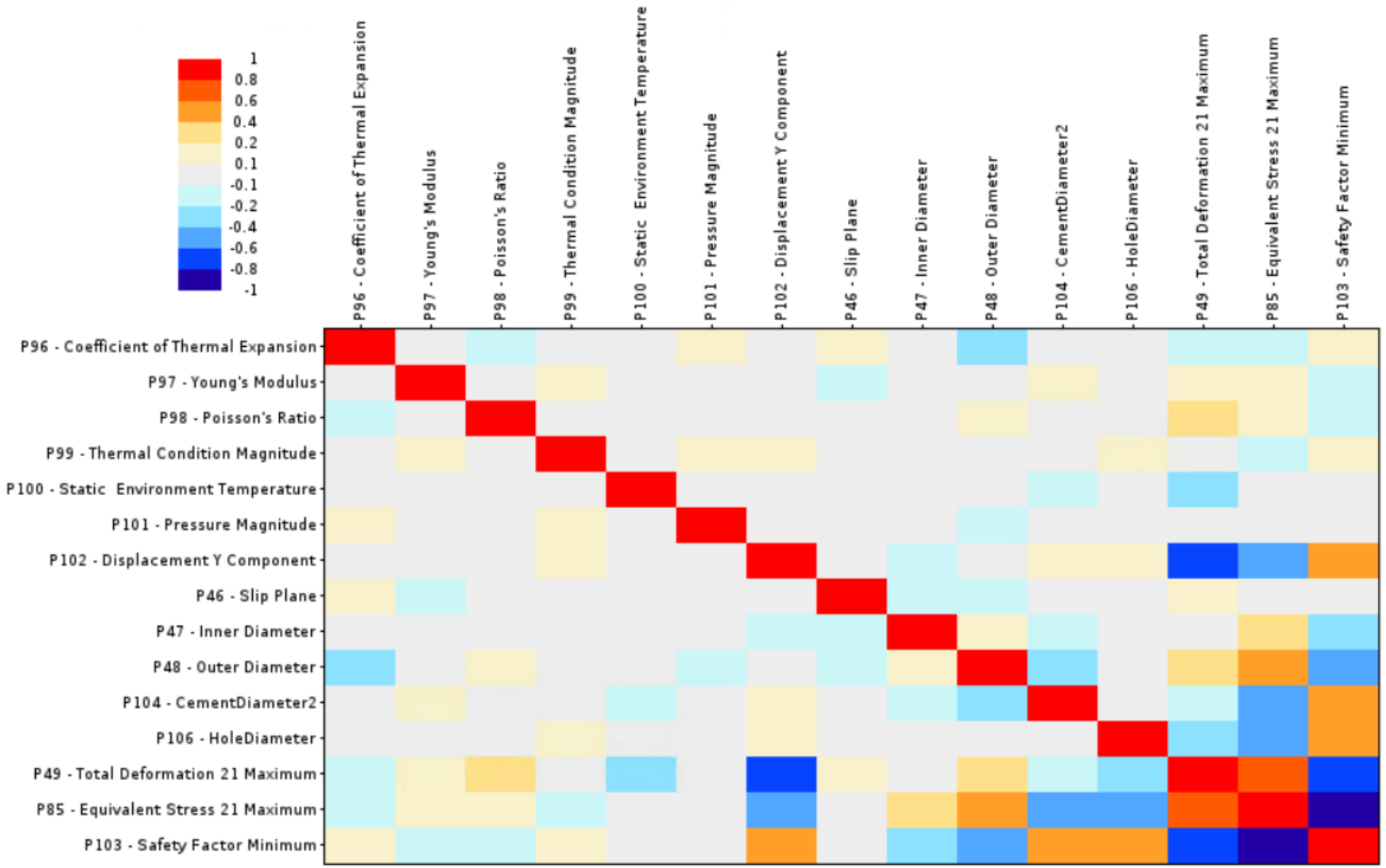

Figure 12 Correlation matrix showing the correlation between the 12 input and 3 output parameters

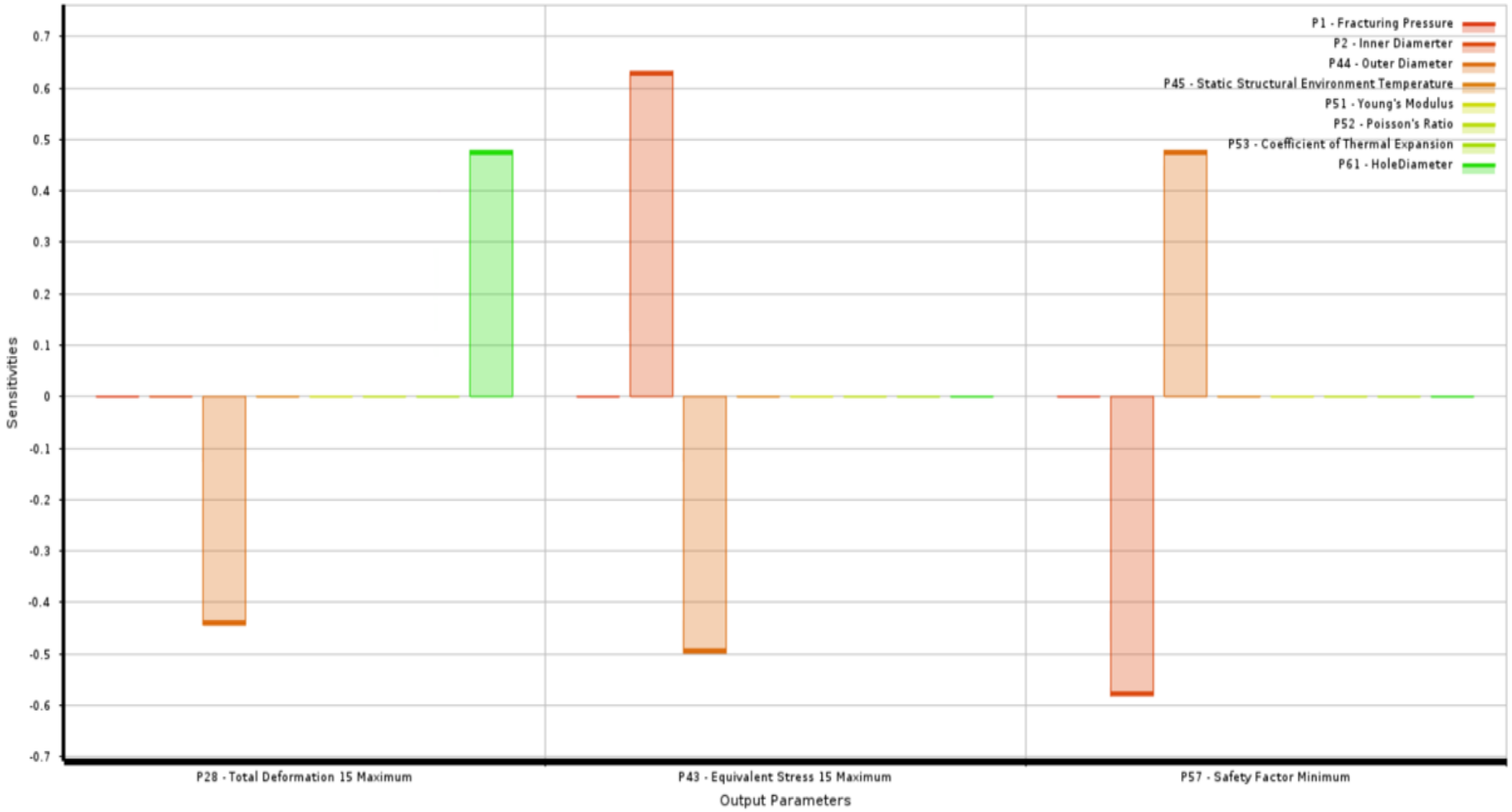

Figure 13 Local sensitivities of input parameters on casing total deformation, von Mises stress and safety factor.

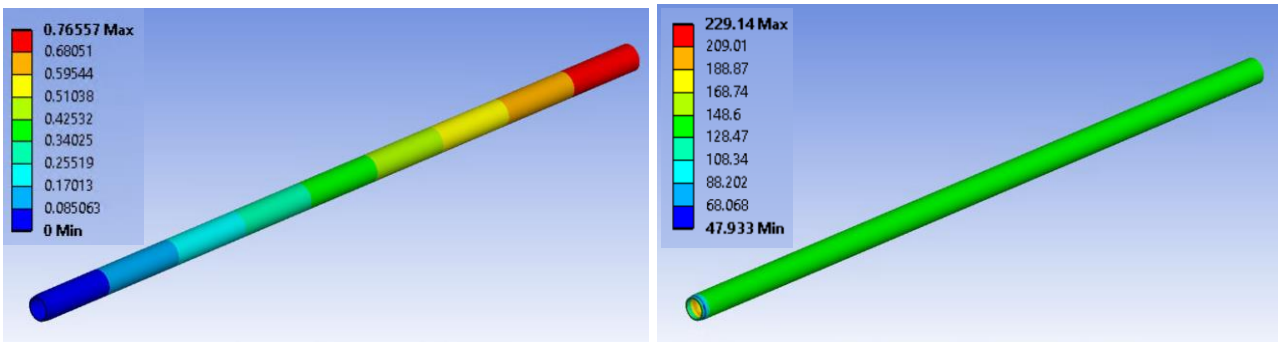

Figure 14 Total deformation and von Mises stress for the optimised design

The optimise results presents three candidates design that meet all the objectives and constraints. Figure 14 presents a sample contour plots of total deformation and von Mises stress for one of the optimised designs.

The design variables that yielded the optimised von Mises and displacement of 299MPa and 0.76mm on Figure 13 are: 4.08inches (103.632mm) and 5.00 inches (127mm) inner and outer diameter, respectively. Cement elastic modulus and well diameter is 6635MPa and 6.0-inch hole. The fracturing pressure and surface temperature is 32MPa and 25.52°C. On the other hand, fixed parameters or constraints corresponding to this scenario of combined loading of 5.29mm slip displacement during flow back with a thermal load of 143.3°C from the reservoir.

This result agrees with what has been established in literature on limiting the cement elastic modulus to below 10000MPa and reducing the fracturing pressure as pointed by Guo et al. (2018) and Yan et al. (2019) in their respective studies. Besides, a new study by Huang et al. (2020) on rubberise cement established that; the rubberise cement absorb micro expansion and shrinkage, which reduces the brittleness of the concrete and improves its deformation performance.

As it can be seen the total deformation recorded after the optimisation is only 0.7655mm after the 30 hours of combined loading. Also, the computed von Mises stress corresponding to this deformation is 299MPa as shown on Figure 14. This value is below the casing yield strength of 758MPa. As such, based on this result it can be said casing's structural integrity is guaranteed. This gives a safety factor of 3.3 against the previous predicted stress of 932.46 MPa with a safety factor of 0.8129.

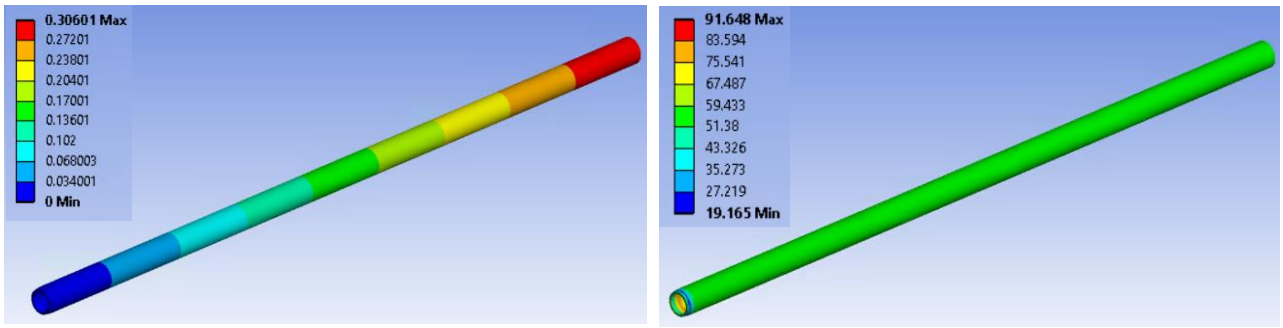

Figure 15 Optimised critical displacement and von Mises after 9 hours of combined loading.

However, if the circumstance change, then a much thicker casing geometry will be needed to cope with the change. Under this example design, 5.29mm slip displacement at an angle of 30 degree to the horizontal axis, 32MPa fracturing pressure and 143.3°C thermal stress will not deform the casing whose internal and outer diameter is 4.08 and 5.00 inches, respectively.

On the other hand, the extracted result after 9 hours of combine loading for displacement and von Mises corresponding to earlier critical simulations results, are shown on Figure 15. This shows a remarkable reduction in the values of the total deformation and von Mises after optimisation. This represents 89% reduction in total deformation compared to initial simulation results.

4.2 Stress prediction using KNN model for casing design accuracy

The significance of this section is to demonstrate the use of KNN machine learning algorithm for the classification and prediction of casing health status, as well as quicker stress prediction than ANSYS. The data utilised comprises of both "buckled" and "intact" scenarios obtained from FEA. The analysis on the simulation data generated classify the casing status into "buckled" and "intact" as shown. Figure 16 presents the scatter plots of the raw simulation data for von Mises plotted against casing inner diameter for the range of 4.5 - 6.625inches diameters (114.3-168.275mm) as shown.

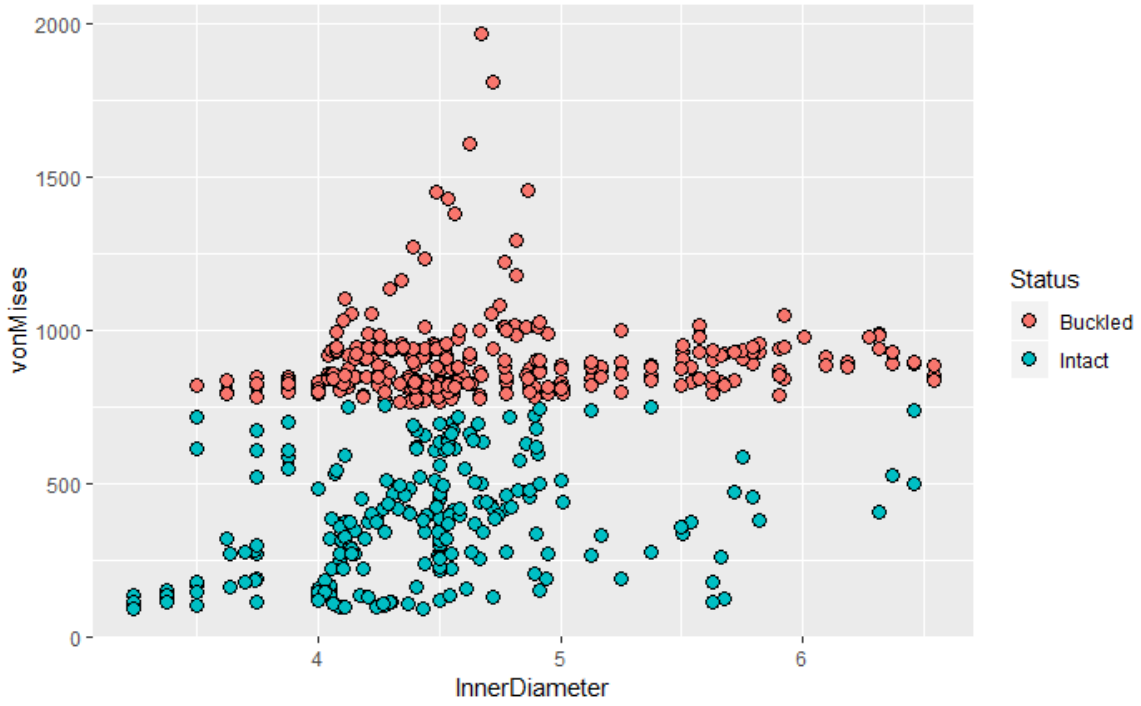

Figure 16 scatter plots showing predicted von Mises stress for different casings geometries (Inner diameter).

Train-control which control the computational variation of the train function is applied for the regression, while the argument of "repeated cross-validation" is selected for the resampling method in this study. The root means square error (RMSE), Rsquared and Mean absolute error (MEA) are used to select the optimal model that gives the result as shown on Table 3. After several trials adjusting the hyperparameter, a model with K= 3 gives the best possible prediction based on

"Rsquared" as shown on Table 3. This gives a metric accuracy of 42.72% as shown on Table 3 for k=3. Also, Table 3 presents "k" values and the corresponding values of RMSE, Rsquared and Mean absolute error (MAE) of the final model.

Table 3 RMSE, Rsquared and MAE for various values of k.

k	RMSE	Rsquared	MAE
1	147.8524	0.4030724	242.8430
2	153.1275	0.4250579	223.7322
3	154.0407	0.4272247	220.5380
4	159.0814	0.4104764	222.5914
5	164.3681	0.4059004	222.5398
6	165.8822	0.4068940	222.5053
7	166.1047	0.4132182	221.5441

Figure 16 presents scatter plots for the prediction of von Mises stress based on the 12 attributes listed in Table 2. It can be seen Figure 17(a) show the scatter plots of actual von Mises stresses against the predicted before fine tuning the hyperparameter. However, after fine tuning of hyperparameter, a significant improvement in prediction accuracy is achieved. This yielded the most improve prediction model shown on Figure 17(b).

Table 4 Variable importance to prediction accuracy on casing buckling phenomena based on KNN algorithm for von Mises stress.

Slip Displacement	100.000000
Outer Diameter	79.673703
Slip Plane	70.206126
Inner Diameter	43.533671
Reservoir Temperature	24.969509
Cement Diameter	22.179621
Cement Modulus	20.701206
Fracturing Pressure	20.174114
Cement Ratio	11.486119
Hole Diameter	10.102478
Ambient Temperature	8.422043
Coefficient of Thermal Expansion	0.000000

Furthermore, the variable importance varies from 0 to 100 is shown on Table 4 based on regression analysis on the data using the KNN algorithm.

The parameters that substantially affects the von Mises stress are slip displacement, casing geometry (inner and outer diameters), hole diameter and cement mechanical properties. This is also true on the correlation matrix on Figure 12 and Lunar (Figure 19). However, coefficient of thermal expansion and ambient temperature do not significantly affect casing structural integrity provided the casing is properly cemented in place. Other factors with their respective influence on the casing von Mises stress are as presented on Table 4.

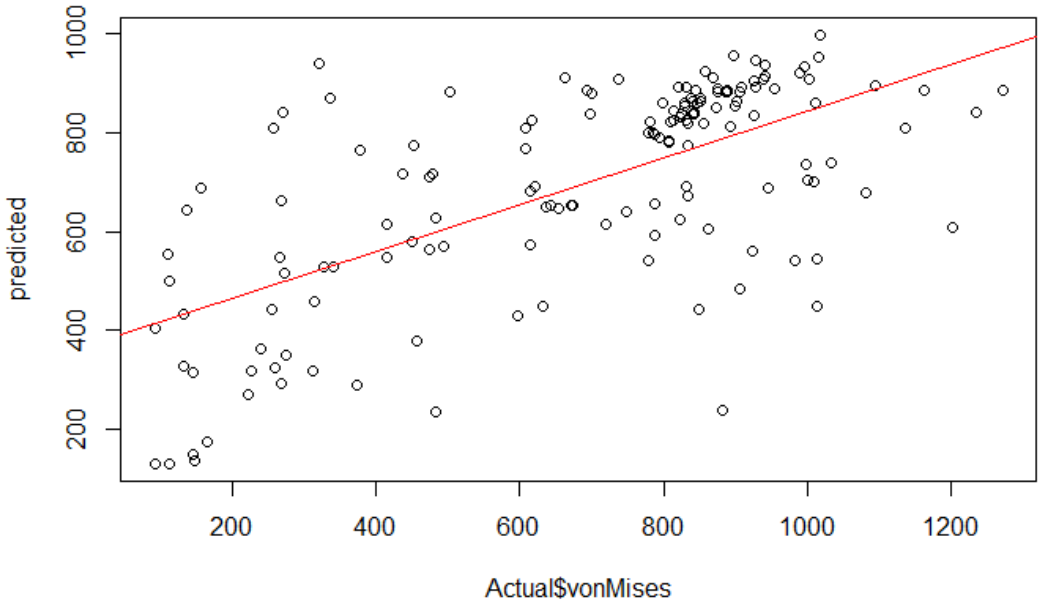

(a)

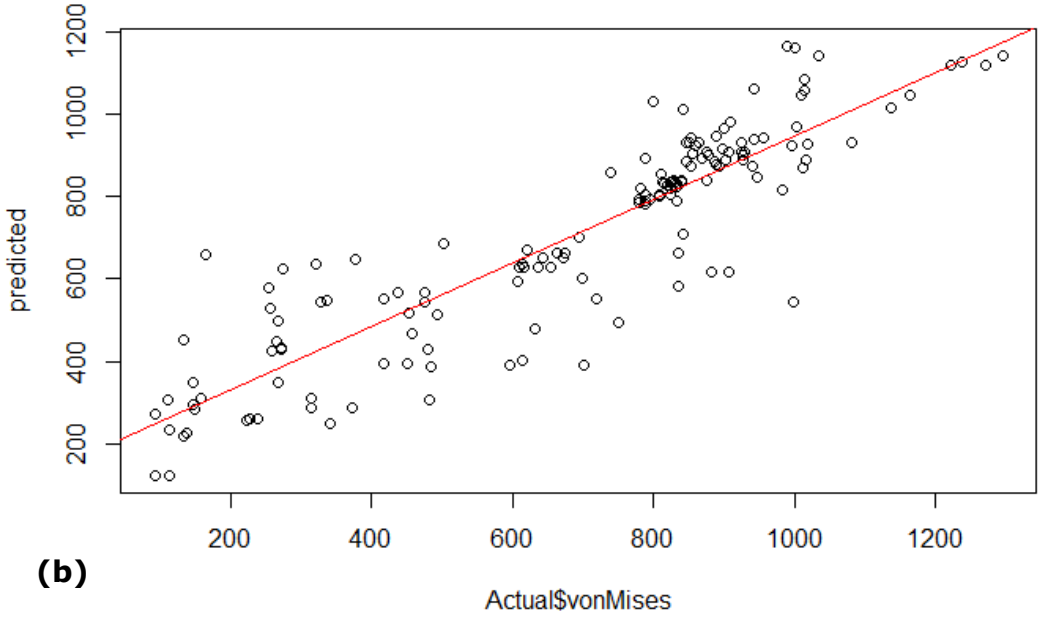

(b)

Figure 17 scatter plot for von Mises stress prediction:(a) before fine-tuning hyper parameter (b) after fine-tuning hyper parameter.

4.3 Effect of slip plane and casing inner diameter on casing stress

Lunar evaluated the effect of changing slip plane and inner diameter on casing von Mises stress over time is examined on the testing dataset (DOE). The (grey shadow) is generated assuming the slip plane and inner diameter were to change 100 times for selection and design purposes.

The analysis in Lunar predicted the corresponding responses for the new design of experiment (DOE). The influence of each parameter is investigated and corridor

of each evaluated. Figure 18(a and b) present the corridor for slip plane and inner diameter respectively on von Mises stress over the period of investigation.

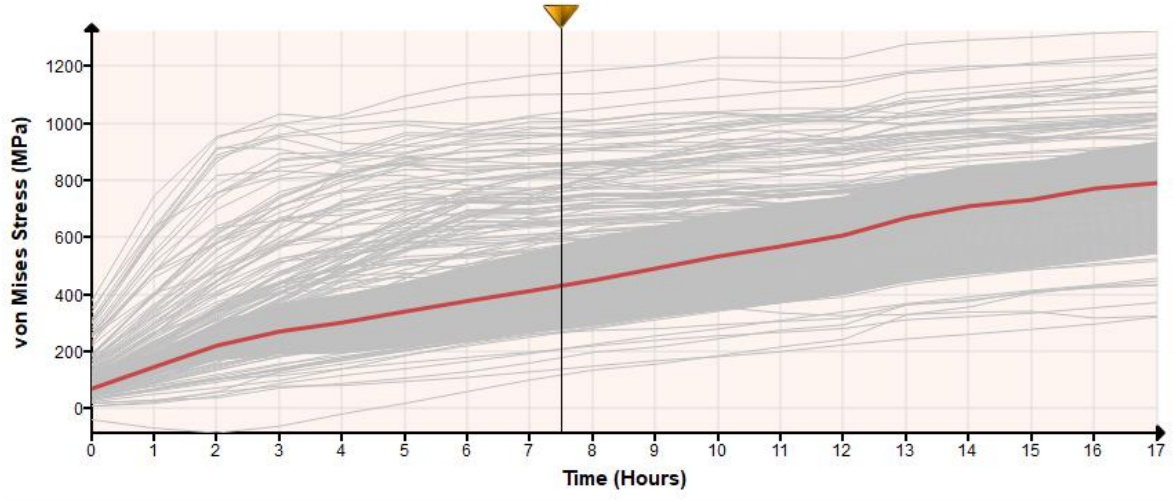

(a)

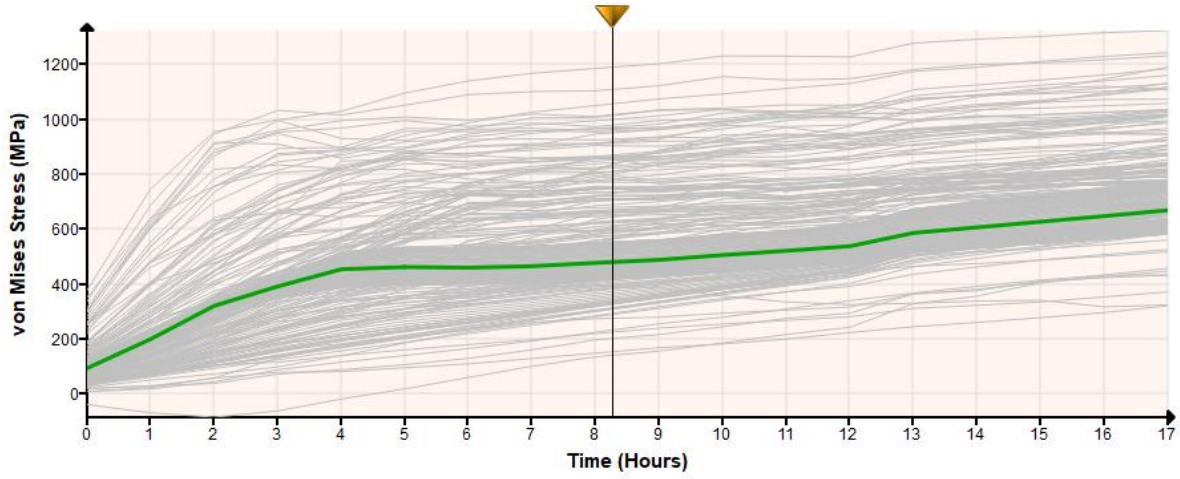

(b)

Figure 18: (a) Effect of changing slip plane 100 times (b) effect changing casing Inner diameter 100 times showing the window in grey over time in each case

As expected, and as it can be seen, different parameters (see Table 4) have different influence on casing von Mises stress particularly for time dependent data as shown on the Figures 18. This is particularly crucial as it allows the engineer to examine range of scenarios for an inform decision within a very short time. As it can be seen on Figure 18(a) the corridor is wider than on Figure 18(b) for slip plane and inner diameter, respectively.

4.4 Effect of design parameters on casing stress performance

The Lunar predicted the influence and the variance/standard deviations of the design parameters on casing structural performance using fraction of the simulation data earlier explain in section 3.2.2. The sensitivities of all parameters are presented on the bar chart plotted on Figure 19. As it can be seen the slip

displacement (SD) has the highest impact on the casing stress. This is obvious and completely agree with variable importance based on KNN metric prediction accuracy shown on Table 4. Other parameters that strongly affect the target variable (von Mises) is slip plane (SP) and inner diameter (ID). Meanwhile, outer diameter (OD), Fracturing pressure (FP), and Poisson's ratio (PR) have very little / no influence on the von Mises stress. However, cement elastic modulus (CEM) and reservoir temperature (RT) affect the casing stress moderately as shown on Figure 19.

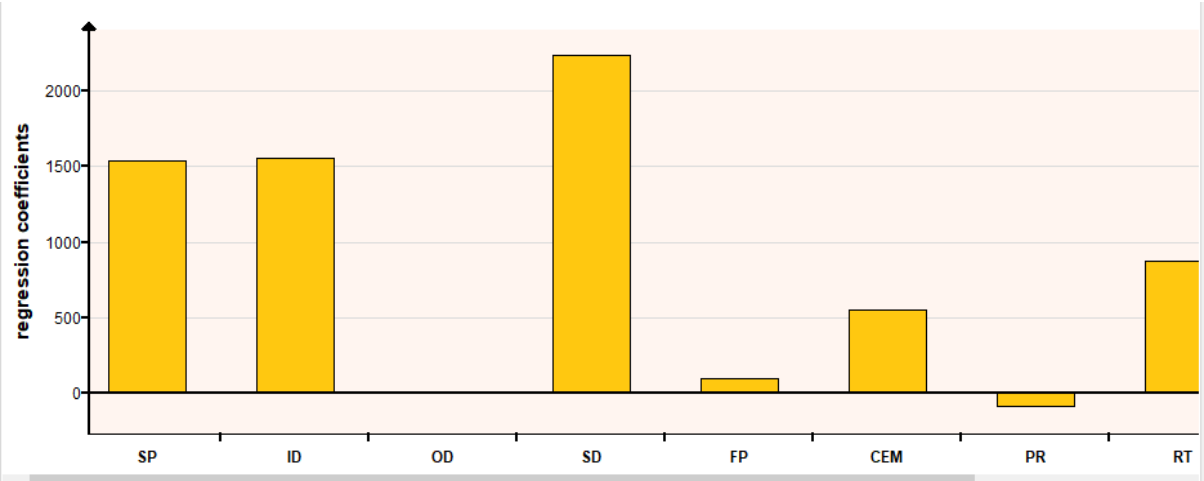

Figure 19 The inputs parameters influence on casing von Mises stress.

The PCA presents the standard deviation between the parameters. As it can be seen on plot the standard deviation ranges from -4 to +4 on both axes. Although, the data is highly variable (imbalance), the PCA show good distribution as shown on Figure 20. On Figure 20, Inner and outer diameter (ID & OD), surface and reservoir temperatures (ST & RT) are strongly correlated.

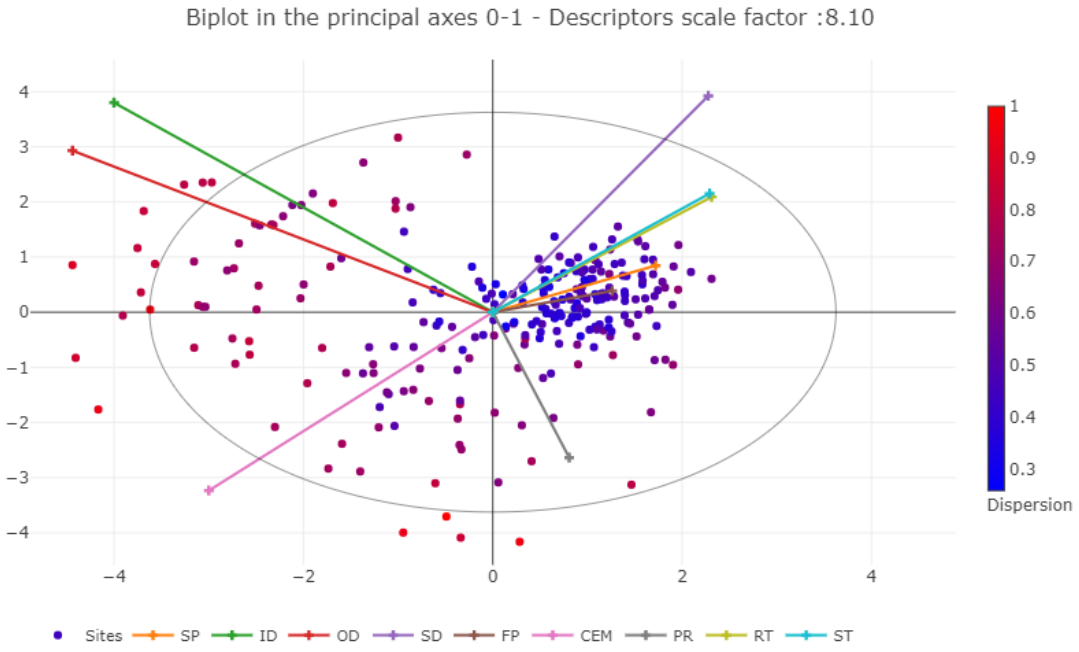

Figure 20 Principal component analysis of the casing performance based on sensitive parameters

Figure 21 presents the variance contribution of each of the 9 parameters under investigation. The gradual diminishing of the bars indicates a good principal component analysis.

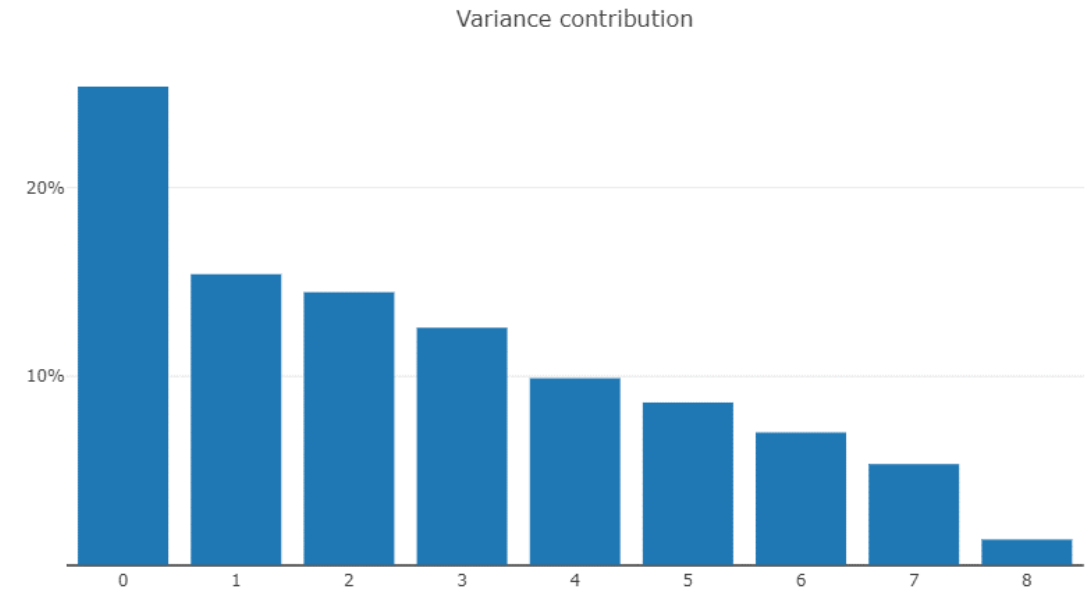

Figure 21 The variance of the contributing sensitive parameters.

4.5 Selection and optimisation for the casing design

The optimisation functionality of Lunar iteratively goes through the design variables to select the right values (bounds) of those parameters that enable the determination of a predetermined casing stress threshold specified by the user. Consequently, Lunar revealed the parameter sets that enable determination of right combination of values that can achieve predetermine target (optimum) without reaching the casings' strength limit. For this purpose, 650MPa was selected as the maximum value for the P110 casing which has a minimum yield strength of 758 MPa. After the analysis, the optimised parameters are presented on Figure 22.

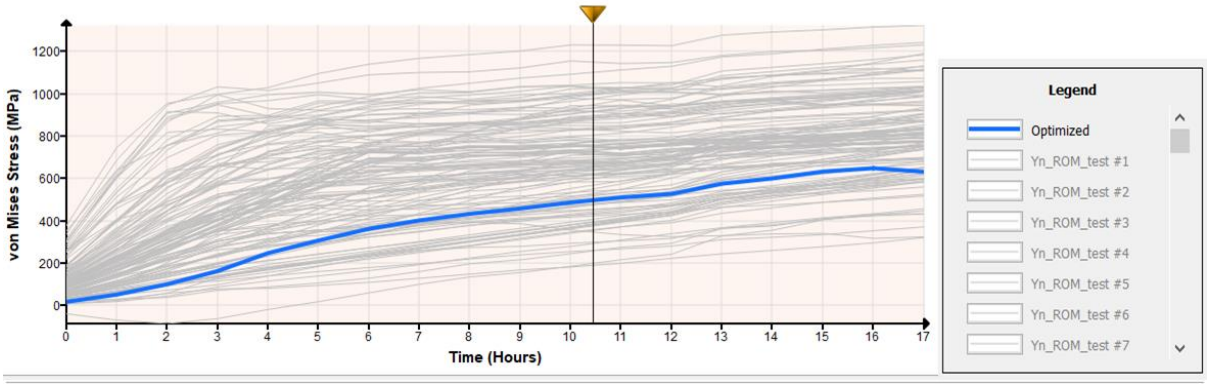

Figure 22 Lunar software output for the optimised casing design shown in blue line.

Under this specific example optimisation with Lunar, limiting the von Mises stress for P110 to 650MPa is shown on Figure 22. This is achieved with a casing geometry of 113.593 and 164.7mm for inner and outer diameter, respectively. Also, the

maximum fracturing pressure of 49.29MPa was computed to meet this objective. Furthermore, cement with 19258.5MPa and 0.39 Poisson's ratio with fluids temperature of 25.24°C are the corresponding design variables for this situation.

However, in keeping this stress level (650MPa) in the casing, the maximum permissible slip displacement is only 2mm on the casing. Also, other fixed variables such as slip plane, and reservoir temperature are 41 degrees and 133.1°C, respectively. This agrees with the previous study of Yin et al. (2018) and Xi et al. (2018) that established low slip angle reduce buckling tendencies.

The heatmap presents the von Mises distribution for the 18th column which corresponds to the 10th hour casing responses under the combined loading. It is showing the distribution of the von Mises stress for this particular column to varies between 200- 1200MPa as shown on the scale.

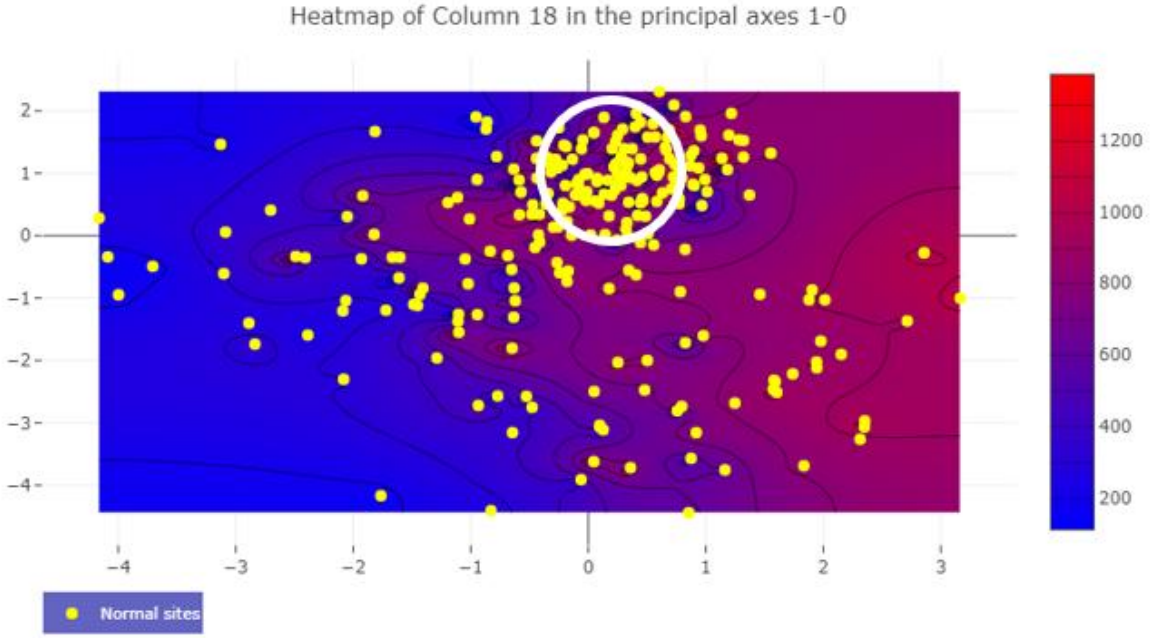

Figure 23 The heatmap for the 10th hour von Mises stress for the optimised casing

It indicates low and high regions for this particular column as shown by the left and right extremes of the heatmap on Figure 23. It is important to point that the optimal region resides where there is high density cluster (circled region) in the middle. From the analysis accomplished in this study, both Lunar and Quasar results have proved to be an effective tool that can optimise the casing selection, design and completion of shale gas horizontal wells.

In summary, investigation of casing structural responses under various slip displacements and a wide range of scenarios between reservoir and surface temperatures, fracturing pressures, casing geometries and downhole conditions and optimisation performed. However, this investigation is limited to induced stresses resulting from slip displacements - during flowback and fracturing pressures in hydraulic fracturing operations and thermal loads for a 30-hour period. In addition, this investigation covers many conditions but limited to the range of parameters and magnitude indicated on Table 2. In particular, cement

elastic modulus magnitude is restricted from 6500 to 10000MPa as established by literature.

A quick comparison between the two approaches on the sensitivities of the casing structural responses - specifically the von Mises stress is summarised in Table 5. As it can be seen, there is good agreement between Lunar and KNN" on most of the parameters investigated. Slip displacement, Inner diameter and slip plane appears to have highest influence on the casing stress based on their magnitude. On the other hand, cement coefficient of thermal expansion, fracturing pressure and Poisson's ratio have low impact on the casing stress magnitude. Although, the two approaches do not use the same amount of data, yet good trend has been established in terms of the sensitivities with the exception of outer diameter which appears to be unique. This is partly due to the constant nature of the outer diameter within a particular casing geometry group.

Table 5 presents this comparison between Lunar and "KNN" sensitivities on casing stress.

Parameter	Lunar	KNN
Slip Displacement	2300	100
Outer Diameter	0	79.6737
Slip Plane	1580	70.20613
Inner Diameter	1600	43.53367
Reservoir Temperature	800	24.96951
Cement Modulus	600	20.70121
Fracturing Pressure	100	20.17411
Poisson's Ratio	-100	11.48612
Coefficient of Thermal Expansion	0	0

5 Conclusion

This paper proposes a novel way to investigate and optimise the casing structural integrity using two approaches of finite element analysis (FEA) and machine learning. The approach in this study is unique, as it is able to capture the pertinent parameters influencing the casing buckling and the evaluation of the magnitude of each. In this work, the effect combined loading using multiple parameters to establish the relationship and effect of each on stress, displacement and ultimately casing safety factor is revealed. Similar approaches of combining machine learning and FEA are established in the study of Kim, M., Yi, S. and Hong, S., (2021) which, acquire a training data for machine learning from 100 simulations to determine an optimal design. Also, Sabanci, K., (2020) applied Machine learning and FEA to carry-out parametric simulation and modelling of brushless Direct Current motor (BLDC).

Simulation results for the combined loading of slip displacement and thermal loading when the fracture slip plane is 60° reveal casing transverse displacement and von Mises stress to be 13.029 mm and 932.46 MPa respectively after 30 hours. Similarly, the critical stress and displacement computed after 9 hours of combined loading is found to be 759.07MPa and 3.0529mm, respectively.

The optimised result on the other hand, the total deformation and the von Mises recorded after the optimisation is only 0.7655mm and 229MPa after the 30 hours

of combined loading, respectively. Also, the extracted critical results after optimisation represent over 89% reduction in total deformation and 87% reduction in von Mises compared to initial simulation results.

Data mining using Lunar and Quasar provided major insights into the casing health status and enabled the real time parametric investigation of the casing stress. The KNN algorithm prediction gives a metric accuracy of 42.72% based on Rsquared for k=3. The algorithm presents variable significance to casing buckling phenomena with slip displacement and casing geometry (inner and outer diameters) accounting for the larger proportions. Using Lunar and the KNN prediction model, one can quickly determine the von Mises stress under a given scenario similar to those shown in Table 3 in order to make an inform decision. Therefore, adopting to this procedure in casing design for shale gas wells will drastically reduce the potentials of casing buckling as established in this study.

Acknowledgement:
We would like to acknowledge financial funding by Petroleum Technology Development Fund (PTDF- Abuja Nigeria) under its overseas scholarship scheme for Auwalu Mohammed PhD scholarship. Grant Reference Number: PTDF/ED/PHD/MAI/1048/17. We would also like to acknowledge CADLM for permission to use their commercial software (ODYSEE) to accomplish some of the tasks in this study.

References

Bachu, S. 2017, "Analysis of gas leakage occurrence along wells in Alberta, Canada, from a GHG perspective–Gas migration outside well casing", *International journal of greenhouse gas control,* vol. 61, pp. 146-154.

Bao, X. & Eaton, D.W. 2016, "Fault activation by hydraulic fracturing in western Canada", *Science (New York, N.Y.),* vol. 354, no. 6318, pp. 1406-1409.

Bartlett, M. & Cussens, J. 2017, "Integer linear programming for the Bayesian network structure learning problem", *Artificial Intelligence,* vol. 244, pp. 258-271.

Carpenter, C. 2019, "Data Mining Effective for Casing-Failure Prediction and Prevention", *Journal of Petroleum Technology,* vol. 71, no. 07, pp. 55-56.

Cussens, J., Järvisalo, M., Korhonen, J.H. & Bartlett, M. 2017, "Bayesian network structure learning with integer programming: Polytopes, facets and complexity", *Journal of Artificial Intelligence Research,* vol. 58, pp. 185-229.

Donoho, D.L. 2000, "High-dimensional data analysis: The curses and blessings of dimensionality", *AMS math challenges lecture,* vol. 1, no. 2000, pp. 32.

Duda, R.O., Hart, P.E. & Stork, D.G. 2012, *Pattern classification,* John Wiley & Sons.

Fan, G., Guo, Y., Zheng, J. & Hong, W. 2019, "Application of the weighted k-nearest neighbour algorithm for short-term load forecasting", *Energies,* vol. 12, no. 5, pp. 916.

Guo, X., Li, J., Liu, G., Lian, W., Zeng, Y., Tao, Q. & Song, X. 2018, "Shale experiment and numerical investigation of casing deformation during volume fracturing", *Arabian Journal of Geosciences,* vol. 11, no. 22, pp. 723.

Haghshenas, A., Hess, J. & Cuthbert, A. 2017, "Stress analysis of tubular failures during hydraulic fracturing: cases and lessons learned", *SPE Hydraulic Fracturing Technology Conference and Exhibition* Society of Petroleum Engineers.

Huang, Z., Deng, W., Du, S., Gu, Z., Long, W. and Ye, J., 2020. Effect of rubber particles and fibers on the dynamic compressive behaviour of novel ultra-lightweight cement composites: Numerical simulations and metamodeling. *Composite Structures*, p.113210.

Jabbar, M.A., Deekshatulu, B.L. & Chandra, P. 2015, "Classification of heart disease using k-nearest neighbour and genetic algorithm", *arXiv preprint arXiv:1508.02061.*

Jacobs, T. 2020, "An Unconventional Challenge Can Casing Failures During Hydraulic Fracturing Be Stopped?", *Journal of Petroleum Technology,* vol. 72, no. 01, pp. 26-32.

Kayvantash, K. 2015-2019, "ODYSSEE: Optimal Decision Support System for Engineering and Expertise", a ML/ROM based AI software platform for real-time predictions and optimization.

Kim, M., Yi, S. and Hong, S., 2021. Numerical Investigations on the Shape Optimization of Stainless-Steel Ring Joint with Machine Learning. *Applied Sciences*, *11*(1), p.223.

Li, Y., Liu, W., Yan, W., Deng, J. & Li, H. 2019, "Mechanism of casing failure during hydraulic fracturing: Lessons learned from a tight-oil reservoir in China", *Engineering Failure Analysis,* vol. 98, pp. 58-71.

Lian, Z., Yu, H., Lin, T. & Guo, J. 2015, "A study on casing deformation failure during multi-stage hydraulic fracturing for the stimulated reservoir volume of horizontal shale wells", *Journal of Natural Gas Science and Engineering,* vol. 23, pp. 538-546.

Liang, X., Zhu, J., Shi, X., Zhang, J., Liu, C., He, F. & Li, R. 2017, "Staged fracturing of horizontal shale gas wells with temporary plugging by sand filling", *Natural Gas Industry B,* vol. 4, no. 2, pp. 134-140.

Liu, K., Gao, D., Wang, Y. & Yang, Y. 2017, "Effect of local loads on shale gas well integrity during hydraulic fracturing process", *Journal of Natural Gas Science and Engineering,* vol. 37, pp. 291-302.

Liu, K., Dahi Taleghani, A. and Gao, D., 2020. Semi analytical model for fault slippage resulting from partial pressurization. *SPE Journal*, *25*(03), pp.1-489.

Liu, W., Yu, B. & Deng, J. 2017, "Analytical method for evaluating stress field in casing-cement-formation system of oil/gas wells", *Applied Mathematics and Mechanics,* vol. 38, no. 9, pp. 1273-1294.

Mainguy, M. & Innes, R. 2019, "Explaining Sustained" A"-Annulus Pressure in Major North Sea High-Pressure/High-Temperature Fields", *SPE Drilling & Completion,* vol. 34, no. 01, pp. 71-80.

Mitchell, T.M. 2006, *The discipline of machine learning,* Carnegie Mellon University, School of Computer Science, Machine Learning ….

Mohammed, A.I., Oyeneyin, B., Atchison, B. & Njuguna, J. 2019, "Casing structural integrity and failure modes in a range of well types-a review", *Journal of Natural Gas Science and Engineering.*

Mohammed, A.I., Oyeneyin, B., Bartlett, M. & Njuguna, J. 2020, "Prediction of casing critical buckling during shale gas hydraulic fracturing", *Journal of Petroleum Science and Engineering,* vol. 185, pp. 106655.

Prasatha, V.S., Alfeilate, H.A.A., Hassanate, A.B., Lasassmehe, O., Tarawnehf, A.S., Alhasanatg, M.B. and Salmane, H.S.E., 2017. Effects of Distance Measure Choice on KNN Classifier Performance-A Review. *arXiv preprint arXiv:1708.04321*.

Sabanci, K., 2020. Artificial intelligence-based power consumption estimation of two-phase brushless DC motor according to FEA parametric simulation. *Measurement*, *155*, p.107553.

Talebi, R., Ghiasi, M.M., Talebi, H., Mohammadyian, M., Zendehboudi, S., Arabloo, M. & Bahadori, A. 2014, "Application of soft computing approaches for modelling saturation pressure of reservoir oils", *Journal of Natural Gas Science and Engineering,* vol. 20, pp. 8-15.

Theodoridis, S. 2015, *Machine learning: a Bayesian and optimization perspective,* Academic Press.

Wang, H. 2016, "Numerical investigation of fracture spacing and sequencing effects on multiple hydraulic fracture interference and coalescence in brittle and ductile reservoir rocks", *Engineering Fracture Mechanics,* vol. 157, pp. 107-124.

Xi, Y., Li, J., Liu, G., Cha, C. & Fu, Y. 2018, "Numerical investigation for different casing deformation reasons in Weiyuan-Changning shale gas field during multistage hydraulic fracturing", *Journal of Petroleum Science and Engineering,* vol. 163, pp. 691-702.

Xi, Y., Li, J., Liu, G., Cha, C. & Fu, Y. 2018, "Numerical investigation for different casing deformation reasons in Weiyuan-Changning shale gas field during multistage hydraulic fracturing", *Journal of Petroleum Science and Engineering,* vol. 163, pp. 691-702.

Xi, Y., Li, J., Liu, G., Li, J. & Jiang, J. 2019, "Mechanisms and Influence of Casing Shear Deformation near the Casing Shoe, Based on MFC Surveys during Multistage Fracturing in Shale Gas Wells in Canada", *Energies,* vol. 12, no. 3, pp. 372.

Xing, Y., Zhang, G., Lin, Q., Bu, X., Da, Y. & Qi, Y. 2017, "Subcritical fracture process of sandstone with AE energy analysis", *51st US Rock Mechanics/Geomechanics Symposium* American Rock Mechanics Association,.

Yu, H., Dahi Taleghani, A., Lian, Z. & Lin, T. 2019, "Impact of Asymmetric Stimulated Rock Volume on Casing Deformation in Multi-Stage Fracturing; A Case Study", *SPE Annual Technical Conference and Exhibition* Society of Petroleum Engineers.

Zhang, F., Jiang, Z., Chen, Z., Yin, Z. and Tang, J., 2020. Hydraulic fracturing induced fault slip and casing shear in Sichuan Basin: a multi-scale numerical investigation. *Journal of Petroleum Science and Engineering*, *195*, p.107797.